Water permeability, water retention and microstructure of unsaturated compacted Boom clay

E. Romero *, A. Gens, A. Lloret

Department of Geotechnical Engineering and Geosciences, Universidad Politécnica de Catalunya, Jordi Girona 1–3, Mod. D-2 08034 Barcelona, Spain

Abstract

Three classes of experiments are considered in this paper to provide information for two artificially prepared Boom clay fabrics: mercury intrusion/extrusion tests; main wetting/drying paths; and water inflow/outflow transient (permeability) tests. These tests, which are usually treated separately, are joined in a common reference frame to provide information about the morphology of the porous medium and factors influencing Boom clay unsaturated hydraulic states with reference to water retention curves and relative water permeability values. The main objective is to interpret mercury intrusion porosimetry results in order to define an entrance pore size region at ca 130 to 180 nm separating intra-aggregate and inter-aggregate zones. This pore size region is further associated to a delimiting zone in the retention curve separating regions of 'intra-aggregate governing suction' at gravimetric water contents lower than 13–15% (gravimetric water content is not affected by mechanical effects) and 'inter-aggregate governing suction' (gravimetric water content is sensible to mechanical actions). This water content is further used to define a threshold zone around a relative water permeability of $k_w/k_{ws} = 0.01$ delimiting a zone of greater water relative permeability from others that present a restricted flow in a generalised Darcian sense. All these results are consistent with the existence of two main pore size regions: an intra-aggregate porosity with quasi-immobile water that is little affected by loading processes and an inter-aggregate porosity for which the loading mechanism results in a reduction of interconnected macropores affecting free water. Testing results show that intra-aggregate water represents between 54 and 59% of the total volume of water in soil in a low-porosity packing compacted at a dry unit weight of 16.7 kN m^{-3}, whereas it corresponds to ca 28 and 38% in the case of a high-porosity packing compacted at a dry unit weight of 13.7 kN m^{-3}. © 1999 Elsevier Science B.V. All rights reserved.

Keywords: Clay; Mercury porosimetry; Pore size distribution; Retention curve; Suction; Water permeability

1. Introduction

The pore size distribution (PSD) obtained by mercury intrusion porosimetry (MIP) is an essential fabric element, which is related with some soil behaviour characteristics: water, air and heat conductivity properties; adsorption and desorption isotherms (capillary phenomena); and distortion and volumetric deformations (rearrangement of fabric units). Predictive equations for saturated permeability based on PSDs are presented in Garcia-Bengochea et al. (1979) (capillary and hydraulic-radius models) and Juang and Holtz (1986) (probabilistic model). Delage and Lefebvre (1984) used the porosimetry technique to investigate fabric changes of a sensitive natural clay during consolidation and to define an entrapped

---

* Corresponding author. Fax: +34-93-4017251.
E-mail address: dromero@etseccpb.upc.es (E. Romero)

and free porosity on clay structure, Griffiths and Joshi (1989) studied changes in PSDs due to consolidation of different clay types, and Al-Mukhtar (1995) analysed pore space results on a kaolinite clay relative to the effects of mechanical and hydraulic states. Prapaharan et al. (1985) predicted the soil moisture characteristic curve of a compacted clay up to a matric suction value of 0.7 MPa based on the porosimetry data.

MIP data is used in this paper to provide information about the morphology of the porous medium related to entrapped and free porosity proportions and about factors influencing Boom clay unsaturated hydraulic states with reference to the soil water retention curve and the relative water permeability. Constant volume main retention curves obtained by vapour equilibrium and air overpressure techniques, as well as MIP data assimilated to the desorption path of the soil moisture characteristic curve, are used to examine the density function of the pore structure for the different artificially prepared clay fabrics. Further results obtained under controlled matric suction using transient inflow/outflow data and interpreted with a diffusion equation are compared to relative water permeability determinations using MIP data calculated by integration over the contributions from filled pores. Relative water permeability is studied as a function of the degree of saturation and for different constant porosity values to define a region separating a zone of greater values from others that present a restricted flow.

2. Material and test procedures

2.1. Soil characteristics and sample preparation

Laboratory tests were conducted on artificially prepared (dry side statically compacted) powder obtained from natural Boom clay (Mol, Belgium). This moderately swelling clay (20–30% kaolinite, 20–30% illite, 10–20% smectite) has a liquid limit of $w_L = 56\%$, a plastic limit of $w_P = 29\%$ and 50% of particles $< 2\,\mu m$. In preparing specimens, powder (passing No. 40–425 μm) is left in equilibrium with the laboratory atmosphere at an average relative humidity of 47% (total suction of ca $\psi =$

100 MPa) to achieve a hygroscopic water content of somewhat <3%. For samples used within the air overpressure technique for matric suction control, the required quantity of demineralised water to achieve a predetermined gravimetric water content of $(15.0 \pm 0.3)\%$ was added to the powder, previously cured at a relative humidity of 90%. After equalisation, it approximately corresponds to an initial total suction of ca 2.3 MPa. This initial water content represents a reasonable value for the workability of the clay powder on the dry side of optimum and does not involve a large suction change when imposing the starting matric suction value of 0.45 MPa.

A variable peak stress–constant stroke static compaction procedure has been followed until a specified final volume is achieved under constant water content. Net vertical stress over air pressure $(\sigma_v - u_a)$ and dry unit weight relationships for specified water contents are plotted in Fig. 1. Each curve terminates at a specific degree of saturation and when reaching near saturated states, the static compaction test is no longer possible and is stopped before the beginning of consolidation. Total suction values determined from vapour equi-
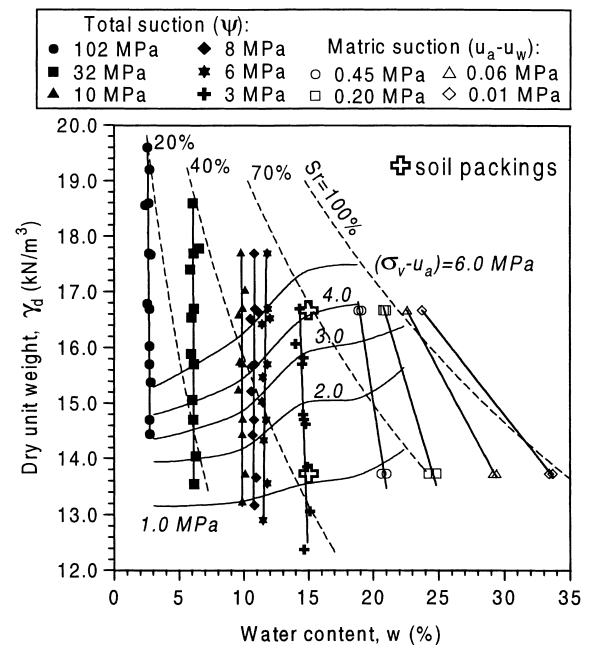

Fig. 1. Static compaction curves with contours of equal suction.

librium technique and matric suction components imposed by air overpressure technique are also represented. A striking aspect is the variation of the degree of saturation upon loading without appreciable change in soil suction, as it is observed in the vertical contours of equal suction represented in this figure, where no important water content change is observed upon loading at suction values higher than $\psi = 3$ MPa. The loading mechanism affects mainly the macroporosity that does not contain free water, because moisture at these fabrication humidity values is mainly adsorbed and held in the less bonded diffuse-layers (i.e. intra-aggregate water, with small quantities at inter-aggregate scale, as further discussed). This way, degree of saturation changes are only associated to macroporosity changes under constant intra-aggregate water content. As matric suction values approach the saturation line, contours of equal suction try to incline in order to converge to this limit condition (the loading mechanism affects inter-aggregate water).

The testing program has included two main soil packings of clay aggregates fabricated at a mould-ing water content of 15%: high-porosity with collapsible tendency structure at a dry unit weight of $\gamma_d = 13.7$ kN m^{-3} and a low-porosity structure with swelling tendency at $\gamma_d = 16.7$ kN m^{-3}, as suggested from matric suction controlled tests reported by Romero (1999). Fabrication preconsolidation net vertical stress is ca 4.5 MPa for the high-density fabric and ca 1.2 MPa for the low-density packing, as indicated in Fig. 1. A qualitative observation with image analysis of scanning electron microscopy (SEM) that complements the overall description of both packings is given in Fig. 2, where local enlargements represented in black and interconnecting clay bridges between aggregates are observed. The constricted porosity arises from these clayey bridges and irregularity of the aggregates, which act as 'ink-bottle' necks entrapping the interconnected porosity, as suggested by Delage and Lefebvre (1984). At higher compressive stresses, the aggregates are fused due to inter-aggregate porosity collapse as shown in Fig. 2(a).

2.2. Experimental methods and procedures

Three major classes of experiments were considered for both soil fabrics: MIP tests; main retention wetting/drying paths; and water inflow/outflow transient tests. MIP tests were carried out on a 'Quantachrome-Autoscan 33' porosimeter, where the mercury pressure is raised continuously between 0.17 and 227 MPa (apparent pore diameters from 7 nm to 9 μm) at a pressure built-up rate of 7 MPa min^{-1}, in conjunction with a 'Quantachrome Autoscan' filling apparatus measuring apparent pore diameters up to 135 μm. MIP tests required dehydrated samples measuring $< 3 \times 10^3$ mm^3 (limited by the sample holder and the cell stem volume). Soil samples were previously prepared and compacted at the desired dry unit weights and at constant water content of (15.0 ± 0.3)%. From each compacted sample, MIP specimens were carefully trimmed into cubes, subsequently freeze-dried to remove the pore water and then kept in a desiccator until testing. A plot of the cumulative pore volume distribution normalised by sample dry weight in an intrusion/extrusion cycle for both soil fabrics is
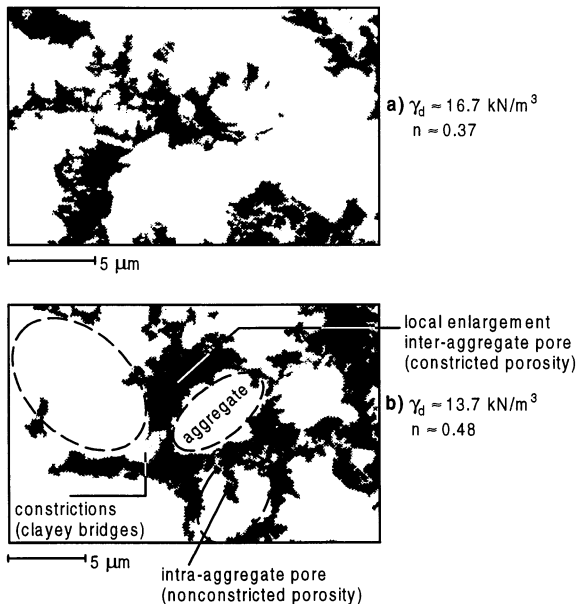

Fig. 2. Image analysis of SEM photomicrographs for the different soil packings. The pores are black and the particles are white.

presented in Fig. 3 (intrusion is represented by the filled symbols). Due to the limited capacity of the microporosity unit to enter the smallest pores, there are some deviations from the theoretical porosity values calculated for the different compacted packings ($\Delta n = 0.020$ for the 13.7 kN m^{-3} packing with an estimated porosity of $n_o = 0.482$ and $\Delta n = 0.029$ for the 16.7 kN m^{-3} fabric with $n_o = 0.371$). This feature confirms the preservation of the soil structure during freeze-drying.

Total suction–gravimetric water content and degree of saturation relationships under free swelling and shrinking conditions with no change in boundary stresses have been measured as a function of the initial dry density (reflecting the different packings), following a multi-stage procedure equilibrated under vapour equilibrium technique (vapour pressure control with different saline solutions), where the same soil specimen undergoes a main wetting phase followed by a main drying stage. Main wetting path refers to the slow water sorption of an initially dry sample at hygroscopic humidity, while first monotonic gradual desorption departing from a minimum suction ever experienced is referred to as main drying. Suction–moisture content relationships were complemented in the lower suction range (between 15 and 2 MPa) using psychrometer data (both transistor and thermocouple in main drying paths). Relationships between total suction and water content at fixed

dry densities have been interpolated from free swelling and shrinking data assuming a nonconstrained intra-aggregate swelling. This term refers to a double-porosity network, where enough space is left at an inter-aggregate scale to allow this swelling (usually for dry densities < 1.7 Mg m^{-3}, where $> 23\%$ of the pore volume corresponds to entrance pore sizes > 1 μm as observed in Fig. 3).

Main wetting and drying data at low suction values (under 0.50 MPa) are obtained from constant volume swelling pressure tests using the air overpressure methodology. Starting from a matric suction of ca 2 MPa the soil is monotonically hydrated up to 0.01 MPa and then is monotonically dried to 0.45 MPa without exceeding the air-entry value of the packing, in order to avoid shrinkage that could alter the null volume condition. Upon wetting, the swelling pressure tests imply certain inter-aggregate porosity decrease at expense of some nonconstrained intra-aggregate swelling in order to maintain the overall constant volume condition. A reasonable correlation has been found between the different values obtained using axis translation and vapour equilibrium procedures. Both techniques can be overlapped in main wetting and drying paths showing the overall
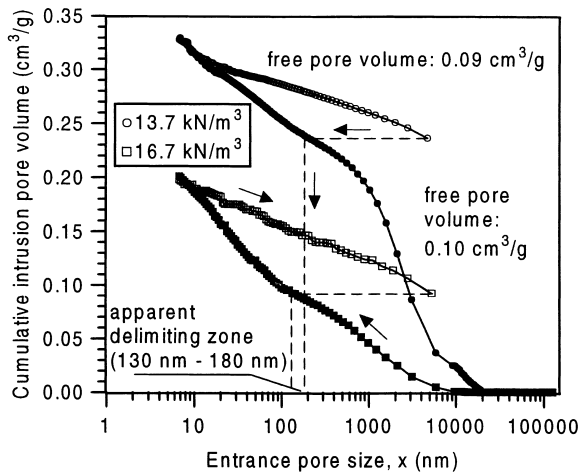

Fig. 3. Cumulative mercury intrusion/extrusion pore volume normalised by the sample weight.
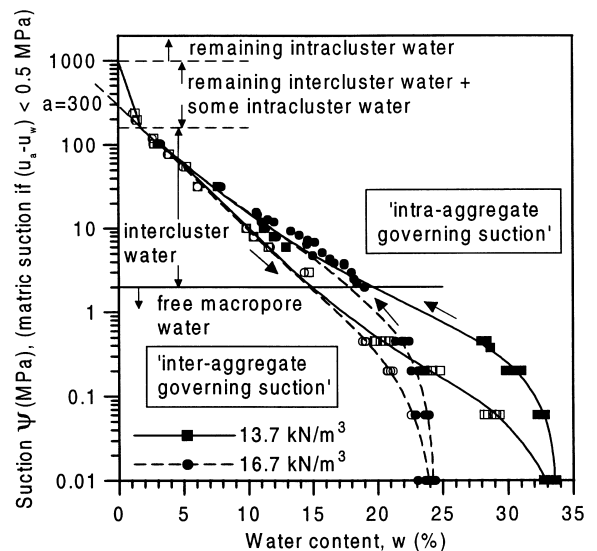

Fig. 4. Main wetting and drying retention curves for the different packings at constant porosity. 'Intra' and 'inter-aggregate governing suction' zones.
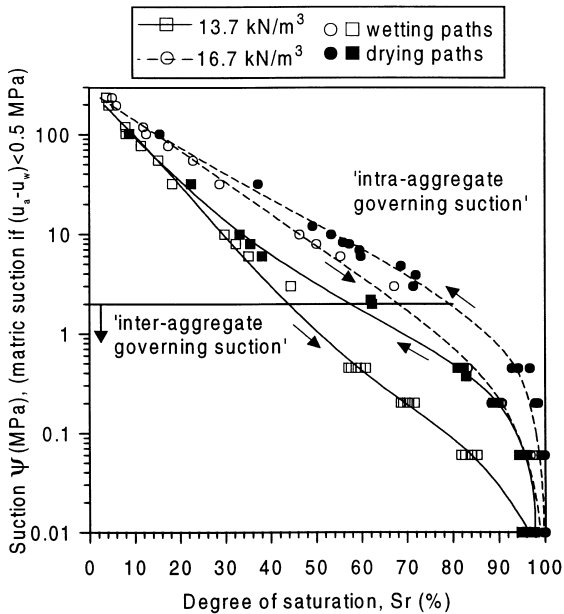
Fig. 5. Suction–degree of saturation retention curves at fixed packings (main wetting and drying paths).

retention curve indicated in Fig. 4. Suction–degree of saturation retention curves at fixed packings represented in Fig. 5 can be estimated by means of volumetric phase relations, where the remarkable influence of clayey soil structure on hysteresis behaviour is observed.

Measurements of the hydraulic conductivity have been performed at different temperatures using oedometer cells under controlled matric suction (both wetting and drying paths) and under constant volume conditions. A step matric suction decrease/increase is applied to the soil and the transient inflow/outflow of water is carefully measured with time and interpreted with the resolution of Richards's diffusion equation taking into account membrane impedance (Kunze and Kirkham, 1962). Experimental problems refer to impedance effects from ceramic disc clogging, diffusion of air into the measuring system and free water evaporation (Romero, 1999).

3. MIP results and interpretations

Two types of porosity can be determined with an intrusion/extrusion cycle (refer to Fig. 3). The

first intrusion fills all the accessible and interconnected pore space, giving the distribution of total porosity, whereas on the complete release of the intrusion pressure it will let only some mercury out from the nonconstricted pores (Delage and Lefebvre, 1984). A second intrusion will follow approximately the same extrusion path, thus defining the free porosity, which seems not to be significantly changed with the increasing compaction effort as observed in the previous figure. Similar results have been reported by Griffiths and Joshi (1989) studying PSD changes due to the consolidation of clay. The difference between the intrusion and extrusion cycle is the entrapped porosity, which accounts for the main reduction in total volume. Delage and Lefebvre (1984) proposed that the free or nonconstricted porosity of the reintrusion volume corresponds to the intra-aggregate pore space, while the inter-aggregate pore space corresponds to the entrapped or constricted porosity. The intra-aggregate porosity detected when pressure is released represents 28% of the total porosity in the low-density packing and accounts for 54% of the total porosity in the high-density fabric, which corresponds to an entrance pore size of ca 130 to 180 nm in the intrusion curve as observed in Fig. 3. This pore size range can be accepted for the delimiting region separating inter and intra-aggregate zones. This pore size region is further utilised to define the 'intra-aggregate governing suction' zone of the retention curve.

MIP results can be used to determine matric suction–saturation relationships at constant packings. The mercury intrusion procedure can become assimilated to a desorption path of the soil moisture characteristic curve in the matric suction range between 0.01 and 45 MPa by applying to an initially saturated sample increasing external air pressure (nonwetting fluid) to gradually dry the soil. Thus the injection of nonwetting mercury with contact angle $\theta_{nw} = 140°$ and interfacial tension $\sigma_{Hg} = 0.484 \, N \, m^{-1}$ is equivalent to the ejection of water from the pores (desorption curve) by the nonwetting front advance of air with $\theta_{nw} = 180°$ for the same diameter of pores being intruded. The volume of pores not intruded by mercury, that is, $Sr = 1 - Sr_{nw}$ ($Sr_{nw} = n/n_o$ stands for the

nonwetting mercury degree of saturation or intruded porosity n normalised by the total porosity n_o), should be used to evaluate the degree of saturation, Sr, corresponding to the equivalent applied air overpressure. However, this last expression does not consider the hygroscopic water content of strongly attracted adsorbed water to the mineral surface and the equivalent residual water content corresponding to the nonintruded porosity. This residual water content corresponds to ca $w_r = 5\%$, which is similar to that obtained in Fig. 4 for a matric suction value of 45 MPa related to the maximum intrusion pressure of 227 MPa. In order to take into account this residual water content, a new expression is proposed: $Sr = (1 - Sr_{nw}) + w_r Sr_{nw}/w_{sat}$, where w_{sat} stands for the saturated gravimetric water content. Fig. 6 represents the main wetting and drying paths for the different soil packings compared to the MIP results. In general, quite a good agreement is observed with respect to the shape of the retention curves, thus being feasible, as a first approximation, to use the cumulative intrusion volume to determine the soil moisture characteristic curve. Similar results were reported by Prapaharan et al. (1985) when analysing on a low suction range the

retention curve based on the MIP data. However, the MIP data follows more closely the wetting paths when they should have come next to the drying paths, which is the moisture curve being predicted. No conclusive explanations have been suggested for these differences, which could arise due to the different effects that water and dissolved salts produce on clay fabric compared to a less active mercury intrusion. However, the rapid desaturation of the high-porosity packing could be related to the fissure like structure detected at ca 10 μm (refer to Fig. 7), which has also been observed by interpreting the porous surface dimension using a fractal scaling of the porosity admitting self-similarity of the hierarchical void structure (Romero, 1999).

Other useful information that can be obtained from the MIP tests is the pore size density function, which is a derivative of the cumulative pore volume represented in Fig. 3. To overcome distortions and emphasised pore sizes, an equally spaced class width on the logarithmic diameter axis of $0.023 < \delta(\log x) < 0.038$ has been selected. The pore size density function at $\log x_m$, evaluated calculating the δSr_{nw} change divided by the change of two adjacent entrance pore diameters reported by the equipment data logger and plotted at the midpoint between those diameters x_m, is presented in Fig. 7. The high-porosity sample appears to
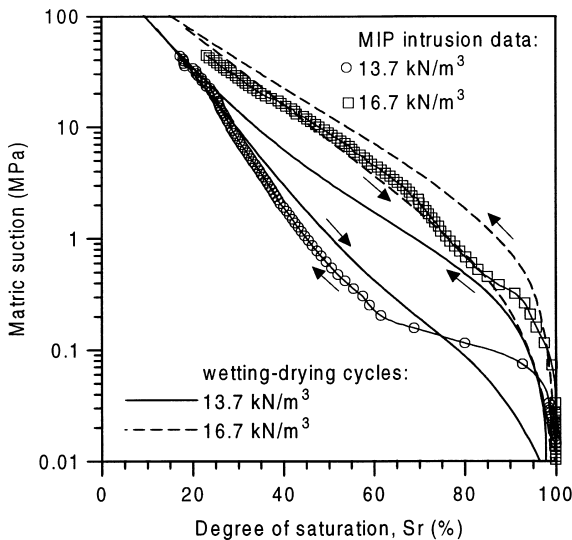

Fig. 6. The main wetting and drying paths on a degree of saturation basis compared to the MIP results for the different packings at constant porosity.
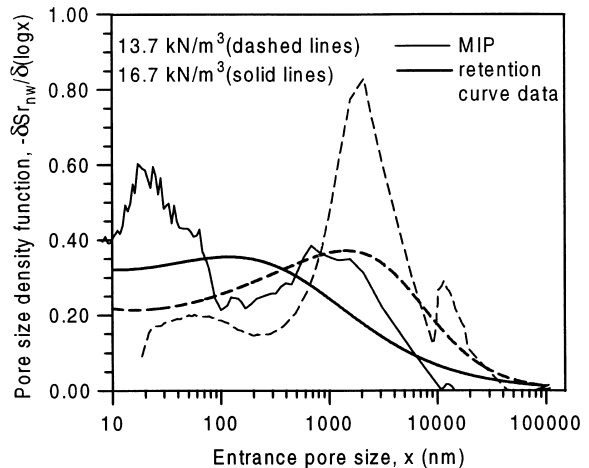

Fig. 7. Pore size density function evaluated from the MIP results and the main wetting retention curve data.

have a trimodal distribution, defining pore modes at ca 10 μm (possibly related to macrofabric fissures), at ca 2 μm (inter-aggregate pore mode) and at ca 50 nm. The low-porosity specimen has a bimodal distribution defined by pore modes at ca 0.7 μm and another at a value of ca 20 nm. As can be observed, changes in soil fabric caused by increasing compaction effort were at the expense of the larger pore modes. Inter-aggregate spaces detected by PSD density functions reveal adequate agreement with SEM images presented in Fig. 2.

4. The main wetting and drying path results and interpretations

At low water content levels corresponding to intra and intercluster water (refer to Fig. 4) the influence of the initial and equilibrated dry densities was found to be negligible, signifying that the suction water content relationship is mainly dependent on the specific surface of the clay (mineralogical composition) and controlled by the soil intra-aggregate microstructure, which will be water-saturated in a main wetting path before the macropores. Under these conditions, a change in density of the soil basically reflects a change in the larger macroscopic voids, which have little influence on water content change and consequently on soil suction. This region, where total suction is insensitive to the degree of saturation changes due to macroporosity reduction upon mechanical loading, is identified in Fig. 4 as 'intra-aggregate governing suction'. This insensitivity is related to the complex and wide nature of clayey soil structure if compared to sands, which present more fix packings. In the suction range between 1000 MPa and ca 2 MPa (for main wetting paths) or ca 5 MPa (for main drying paths), where the overall porosity has little influence on the final water content and where water uptake/intake occurs on an intra-aggregate scale, gravimetric water content appears to be more adequate as a state variable than degree of saturation. Extrapolations to lower suctions may result in different values than measured in suction controlled tests, where different porosity distributions on an inter-aggregate scale are expected for the different packings with multiple-porosity net-

works. Similar observations have been made on compacted sand–bentonite mixtures by Wan et al. (1995), where experimental data clearly show that total suction can be related to the gravimetric water content even though the data come from specimens showing a wide range of initial densities. Delage et al. (1998a) testing compacted bentonite observed little differences with respect to water content at high suctions between the retention curve at constant volume and the curve under free swelling conditions.

On the other hand, the 'inter-aggregate governing suction' zone indicated in Fig. 4 (the water content is high enough to partly fill the inter-aggregate voids) is sensible to mechanical actions, where the loading mechanism is towards the reduction in macroporosity, affecting bulk water contained in the inter-aggregate pores, while maintaining the intra-aggregate porosity not greatly affected by this effect.

The pore size defined by the MIP results delimiting free and constricted porosity of ca 150 nm is associated to an equivalent matric suction or air overpressure of ca 2 MPa according to the Laplace equation, which establishes a mechanical equilibrium across an interface of liquid and vapour in a pore. This capillary pressure corresponds to a gravimetric water content of ca 15% as stated by main wetting path results indicated in Fig. 4. This water content also appears as a delimiting point in the retention curve, separating regions of 'intra-aggregate governing suction' (water content not affected by mechanical effects) and 'inter-aggregate governing suction' (water content sensible to mechanical actions).

This separation between the inter and intra-aggregate zones indicated previously is not expected to be clearly identified in very high-density packings (ca 2 Mg m^{-3} for this type of clay and somewhat lower in more active clays) with a dominant matrix structure, where the delimiting line is expected to be shifted to lower suction values (the 'inter-aggregate governing suction' zone is assumed to be reduced). When performing a constant volume hydration path on such a heavily dry-side compacted packing, the intra-aggregation swelling is constrained due to the limited inter-aggregate porosity, and the interclus-

ter wetting path will tend to the storage capacity of the matrix structure under low suction values. Under these circumstances, no important hysteretic behaviour upon suction reversal is expected, because of the absence of a well-defined air-entry value in the inter-aggregate zone and only induced by the adsorption hysteretic mechanism on a intra-aggregate scale. Delage et al. (1998b) observed no significant hysteresis in the retention curves of heavily compacted clays, which can be explained in terms of the very dense state of the samples in which quasi-reversible intra-aggregate effects are predominant compared to inter-aggregate capillary phenomena.

With reference to Fig. 5, at high suction values corresponding to the 'intra-aggregate governing suction' zone the wetting paths diverge as a result of the variation in porosity at constant water content, reaching a maximum separation around the zone corresponding to the transition between 'intra' and 'inter-aggregate governing suctions', whereas at lower suctions they converge towards 100%. The end of the main adsorption paths may differ slightly for the different packings because of air entrapment in the soil. The air-entry values of the different drying paths appear as a particular transition zone separating quasi-saturated and unsaturated conditions in the 'inter-aggregate governing suction' zone and influencing hysteresis behaviour, which is shown in the closed loops represented in the figure.

The main-wetting and drying retention curves, both in terms of water content and degree of saturation, have been fitted to a modified form of van Genuchten (1980) expression to smooth the steep behaviour of the intercluster water content zone and to take into account a maximum total suction value of around $a = 300$ MPa under null intercluster and free water content (refer to Fig. 4). This value corresponds to the intersection of the linear relationship between the logarithm of the suction and the intercluster water content with the suction-axis at null water content. It appears that this intersection depends on the specific surface of the clay, resulting in higher values for high-activity clays. Total suction corresponding to zero water content as measured in a standard oven drying technique appears to be essentially the same

for all types of soils as suggested by Fredlund and Xing (1994), where a value slightly below 1000 MPa has been experimentally supported. The curve in this high-suction range corresponding to the remaining intercluster and some intracluster water zone can be approximated by another line, which intersects the suction–intercluster water line in an abscissa corresponding to the residual water content.

The PSD density functions of the different clay fabrics can also be obtained from retention curve data. Pore sizes have been calculated using the Laplace equation and a functional form of the retention curve following a modified expression of van Genuchten (1980) has been adopted to evaluate this function. Fig. 7 shows the pore size density function calculated from the main wetting retention curve data, which presents a closer agreement with the MIP intrusion data according to Fig. 6. The PSD density functions show a peak value ca 2 μm for the high-porosity packing, and a somewhat smaller depressed peak ca 150 nm for the low-porosity fabric, thus presenting the general trend observed in MIP data for the dry-side compression effect in the packing fabrication though only one pore mode is detected.

5. Inflow/outflow tests and interpretations

Relative water permeability is studied as a function of the degree of saturation and for different constant void ratio (e) and temperature (T) values, following the general relation:

$$\frac{k_w}{k_{ws}}\bigg|_{e,T} = S_e^\lambda;$$

$$S_e = \frac{w - w_{res}}{(e/Gs) - w_{res}} = \frac{Sr - (Gsw_{res}/e)}{1 - (Gsw_{res}/e)}, \qquad (1)$$

where k_{ws} is the saturated water permeability for the reference configuration; S_e is the effective saturation ratio that can be evaluated on gravimetric water content or degree of saturation bases; and λ is an empirical constant usually related to the PSD. The subscript 'res' refers to the residual gravimetric water content, which is defined as the

water content at which an increase in the total suction does not produce a significant change and is usually related to the hygroscopic water content. Fig. 8 shows the relative water permeability value as a function of the degree of saturation at a constant void ratio corresponding to the different packings and for different temperatures, where no appreciable temperature effects are observed. The relative permeability values have been fitted to Eq. (1) admitting a residual water content of $w_{res} = 2.2\%$, where a high dependency of λ on soil porosity is detected. In clays with a high percentage of adsorbed water associated to a smaller mobility of water adjacent to the mineral surfaces, the relative water permeability with reference to hygroscopic humidity is drastically reduced (high λ values) if compared with free water dominant fabrics (low λ values). In general, below a water content threshold value of ca 13% the relative water permeability is maintained below 1% as observed from the inflow/outflow data interpreted using Darcy's law and a diffusion equation. This quasi-immobile water content, which separates zones of greater water relative permeability values from others presenting a restricted flow in a generalised Darcian sense, is consistent with the intra and intercluster water content within aggregations of clay particles determined from retention curve and MIP data. Fig. 9 shows the normalised effec-
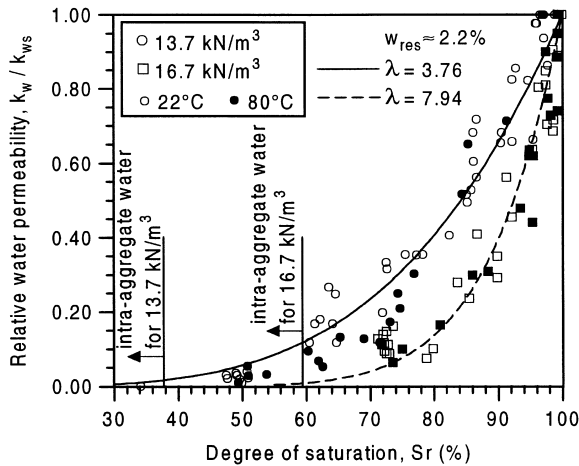

Fig. 8. Relative water permeability–degree of saturation relationships for different packings at constant porosity (inflow/outflow test results).

tive degrees of saturation with respect to this reference cut-off water content, where a parameter of $\lambda = 2.6$ adequately fits the inflow/outflow experimental data corresponding to the different packings.

Relative water permeability appears to be governed by the size and distribution or contribution of interconnected and filled pores within the soil structure, and predictive equations based on PSDs joined to MIP–retention curve relationships permit one to reflect this dependency in terms of the degree of saturation. This way, PSD [in terms of the normalised intruded volume Sr_{nw} at a pressure $p(Sr_{nw})$] or alternatively soil–water characteristic curve data [in terms of the equilibrium degree of saturation Sr at an air overpressure $(u_a - u_w)$] can be used to evaluate the relative water permeability, according to the following expressions:

$$\frac{k_w}{k_{ws}}(x_m) \propto \frac{\displaystyle\int_{x_{min}}^{x_m} x^2 f(x)\,dx}{\displaystyle\int_{x_{min}}^{x_{max}} x^2 f(x)\,dx};$$

$$\frac{k_w}{k_{ws}}(Sr_{nw}) \propto \frac{\displaystyle\int_{Sr_{nw}}^{1} dSr_{nw}/(p(Sr_{nw}))^2}{\displaystyle\int_{0}^{1} dSr_{nw}/(p(Sr_{nw}))^2};$$

$$\frac{k_w}{k_{ws}}(Sr) \propto \frac{\displaystyle\int_{Sr_{res}}^{Sr} dSr/(u_a - u_w)^2}{\displaystyle\int_{Sr_{res}}^{1} dSr_{nw}/(u_a - u_w)^2}, \qquad (2)$$

which assume a porous medium characterised by a pore diameter x and its pore size density function given by $f(x)$, as well as the Hagen–Poiseuille equation for laminar flow through cylindrical capillaries (the permeability is determined by integration over the contribution from the filled pores ranging from x_{min} to x_{max}, with typical MIP values
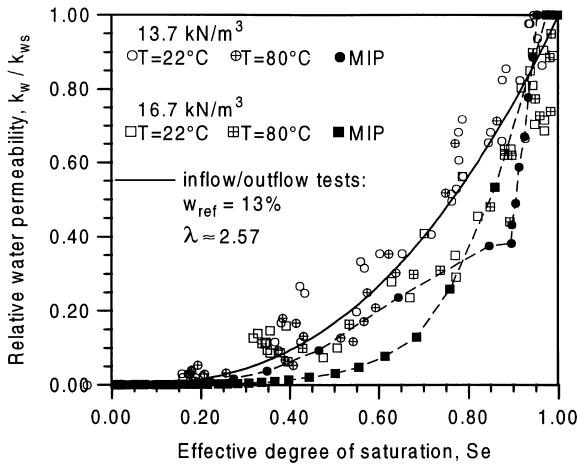
Fig. 9. Relative water permeability–effective degree of saturation for different packings at a reference value of $w_{ref} = 13\%$ (inflow/outflow data and MIP results).

of ca 7 nm to 100 μm). The above expressions consider correlated pores (i.e. the probability of pores of size between x_i and $x_i + dx_i$ on a cross-section i to be connected to pores between x_j and $x_j + dx_j$ in size on the cross-section j is given by $f(x_i)dx_i$ or $f(x_j)dx_j$), though it is obvious that the porous media is extremely disordered and does not fit this concept. Further parameters can be implemented to improve the prediction of the water permeability based on statistical models (Juang and Holtz, 1986; Leong and Rahardjo, 1997).

Relative water permeability values estimated based on the numerical integration of the first expression (2) as a function of the effective degree of saturation (calculated from MIP–retention curve relationships) are represented in Fig. 9, where a similar trend is observed for both packings compared to the relative water permeability values obtained under controlled suction. However, normalised MIP data with respect to a reference quasi-immobile value of $w_{ref} = 13\%$ is shifted towards a somewhat higher value of $\lambda = 4.0$. As observed, estimations from pore volumetric considerations alone cannot be simply related to the relative permeability of the soil, and correction functions to take into account tortuosity of the flow and a partially correlated connection between cross sections are required. Nevertheless, these raw estima-

tions demonstrate the dependency of permeability on MIP and retention curve data, as well as the consequences of porosity and degree of saturation changes.

Macropore free water content at saturation is estimated around $w_{mac} = 9\%$ for the low-porosity fabric presenting a saturated water content of 22% and around $w_{mac} = 21\%$ for the high-porosity packing with a saturated water content of 34%. For saturated Boom clay at a dry unit weight of 16.7 kN m^{-3}, the intra-aggregate quasi-immobile water represents 59% of the total volume of water in soil, whereas it corresponds to 38% in the case of the high-porosity packing. These results compare well with the intra-aggregate porosity determined with mercury extrusion, representing 28% of total porosity in the low-density packing and accounting for 54% of the total porosity in the high-density fabric.

6. Conclusions

The quasi-immobile water fraction (both diffuse-layer and strongly bonded water) contained at the intra-aggregate level can be approximately and indirectly estimated from the MIP (pore size delimiting inter and intra-aggregate zones as indicated in Fig. 3) and main retention curves (inter and nonconstrained intra-aggregate zones as observed in Fig. 4), as well as from relative permeability results (threshold value k_w/k_{ws} ≤ 0.01 delimiting mobile and quasi-immobile water as observed in Fig. 8). In this way, observations of the different microstructural levels detected by these techniques give insight into the understanding of their interrelations from both hydraulic and mechanical viewpoints.

According to MIP intrusion/extrusion results it appears that a pore size of ca 130–180 nm can be accepted as the delimiting value separating inter-aggregate (related to entrapped or constricted porosity) and intra-aggregate (related to free or nonconstricted porosity) zones. This pore size defined by the MIP results is associated to an equivalent matric suction or air overpressure of ca 2 MPa according to the Laplace equation, which corresponds to a gravimetric water content of 15%

as stated by main wetting path results. This water content appears as a delimiting point in the retention curve, separating regions of 'intra-aggregate governing suction' (water content is unaffected by mechanical effects) and 'inter-aggregate governing suction' (water content is sensible to mechanical actions). In addition, a water content of ca 13% is associated to a region that separates zones of greater water relative permeability in a generalised Darcian sense from others which present smaller values. Intra-aggregate quasi-immobile water, calculated from mercury extrusion and relative permeability results, represents between 54 and 59% of the total volume of water in the low-porosity fabric and accounts for ca 28 and 38% in the case of the high-porosity packing. Thus, from approximately one- to two-thirds of water behaves more like a solid than a fluid in these packings.

The MIP data as well as constant volume main retention curves can be used to provide information about the morphology of the porous medium (pore size density function) and about factors influencing Boom clay fabric–property relationships related to unsaturated hydraulic states. In general, reasonable agreement is observed with respect to the shape of the retention curves predicted by the MIP data, although they follow more closely the main wetting paths when they should have come next to the drying paths. Results obtained under controlled suction using transient inflow/outflow data interpreted with a diffusion equation compare relatively well to relative water permeability determinations using the MIP data calculated by integration over the contributions from correlated filled pores. However, further improvements to account for partially correlated connections are required for better relative water permeability predictions.

Acknowledgements

References

Al-Mukhtar, M., 1995. Macroscopic behaviour and microstructural properties of a kaolinite clay under controlled mechanical and hydraulic state. In: Alonso, E.E., Delage, P. (Eds.), Proc 1st Int Conf on Unsaturated Soils vol. 1. Balkema/ Presses des Ponts et Chaussées, Paris, pp. 3–9.

Delage, P., Lefebvre, G., 1984. Study of the structure of a sensitive Champlain clay and its evolution during consolidation. Can. Geotech. J 21, 21–35.

Delage, P., Cui, Y.J., Yahia Aï, M., De Laure, E., 1998a. On the saturated hydraulic conductivity of a dense compacted bentonite, Proc. 2nd Int. Conf. on Unsaturated Soils vol. 1. International Academic Publishers, Beijing, pp. 344–349.

Delage, P., Howat, M.D., Cui, Y.J., 1998b. The relationship between suction and swelling properties in a heavily compacted unsaturated clay. Engineering Geology 50, 31–48.

Fredlund, D.G., Xing, A., 1994. Equations for the soil–water characteristic curve. Can. Geotech. J. 31, 521–532.

Garcia-Bengochea, I., Lovell, C.W., Altschaeffl, A.G., 1979. Pore distribution and permeability of silty clays. J. Geotech. Eng. Div., ASCE 105 (7), 839–856.

van Genuchten, M.Th., 1980. A closed-form equation for predicting the hydraulic conductivity of unsaturated soils. Soil Sci. Soc. Am. J. 44, 892–898.

Griffiths, F.J., Joshi, R.C., 1989. Change in pore size distribution due to consolidations of clays. Géotechnique 39 (1), 159–167.

Juang, C.H., Holtz, R.D., 1986. A probabilistic permeability model and the pore size density function. Int. J. Numer. Anal. Meth. Geomech. 10, 543–553.

Kunze, R.J., Kirkham, D., 1962. Simplified accounting for membrane impedance in capillary conductivity determinations. Soil Sci. Soc. Am. Proc. 26, 421–426.

Leong, E.C., Rahardjo, H., 1997. Permeability functions for unsaturated soils. J. Geotech. Engng., ASCE 123 (12), 1118–1126.

Prapaharan, S., Altschaeffl, A.G., Dempsey, B.J., 1985. Moisture curve of compacted clay: mercury intrusion method. J. Geotech. Engng, ASCE 111 (9), 1139–1143.

Romero, E., 1999. Thermo-hydro-mechanical behaviour of unsaturated Boom clay: an experimental study. PhD Thesis, Universidad Politécnica de Catalunya, Barcelona, Spain (in preparation).

Wan, A.W.L., Gray, M.N., Graham, J., 1995. On the relations of suction, moisture content and soil structure in compacted clays. In: Alonso, E.E., Delage, P. (Eds.), Proc. 1st Int. Conf. on Unsaturated Soils vol. 1. Balkema/Presses des Ponts et Chaussées, Paris, pp. 215–222.